Process Characterization Of Low Temperature Ion Implantation Using Ribbon Beam And Spot Beam On The AIBT iPulsar High Current

Erik J.H. Collart[(1)], Ron Teel[(1)], Charles Free[(1)], Zhimin Wan[(1)], Peter Kopalidis[(1)], M.A. Razali[(2)], Russell Gwilliam[(2)], Andy Smith[(2)], Edward Tsidilkovski[(3)] and Tom Karpowicz[(3)]

[(1)]Advanced Ion Beam Technology, Inc. 81 Daggett Drive, San Jose, Ca 95134, USA, [(2)]Surrey Ion beam Centre, Nodus lab, University of Surrey, Guildford, Surrey GU2 7XH, UK, [(3)]Semilab AMS LLC, 47 Manning Road, Billerica, Ma 01821, USA

Abstract. The damage and amorphous layer formation properties of a 6 keV 1×10^{15} cm^{-2} carbon implant were investigated using spot beam and ribbon beam and substrate temperature. The effects of wafer temperature on dopant activation and diffusion were further investigated for boron implants between 300 eV and 2 keV and arsenic implants between 2 keV and 20 keV. The carbon implant amorphization characteristics can be understood using the concept of critical dose for amorphization. B and As activation was found to be 15%-20% improved at the lowest implant temperature but with similar junction depths compared to higher implant temperatures. Higher energy implants showed less or no activation or junction depth improvement at lower implant temperatures.

Keywords: Ion Implantation, damage, dose rate, cold implant, amorphization
PACS: 85.40.Ry, 61.72.Cc, 61.72.U-

INTRODUCTION

The ion implantation process generates a distinct implant damage signature depending on whether a spot beam or a ribbon beam is used [1]. The wafer temperature during implant will also influence the resultant damage. Next node device requirements place stringent limits on leakage currents and other device parameters affected by the damage formation and annealing. This paper explores this opportunity through the unique capabilities of the AIBT iPulsar high current ion implanter [2]. The iPulsar allows for spot beam as well as ribbon beam tuning on the same tool, with substrate chiller T control down to -50°C.

EXPERIMENTAL

All implants were performed on an Advanced Ion Beam Technology iPulsar high current tool on 300 mm Si wafers with a typical resistivity of 1-25 Ohm.cm. Secondary Ion Mass Spectrometry (SIMS) was carried out using a proprietary PCOR SIMS methodology. HT-XTEM analysis was carried out on a FEI Tecnai G2 F20. RTP steps were done on a Jipelec Jetstar 200ST, in a 10s isochronal scheme from 800°C to 1050°C. Sheet Hall and Rs measurements were performed using an Accent HL5500 on $1cm^2$ samples using the Van der Pauw (VDP) geometry to extract the number of carriers (Ns), their mobility (μ) and corresponding sheet resistance (Rs). The VDP structures were created using standard photolithography and wet chemical etching. Surface Photo Voltage (SPV) measurements were done on a QCS 7300. SPV is a non-contact method based on a surface photo voltage effect and was used to monitor as-implanted damage.

RESULTS AND DISCUSSION

Amorphization Properties Of Carbon

Carbon is used in many advanced process flows in combination with a Ge PAI step and a dopant implant.

The α-layer from the Ge PAI ensures carbon is substitutional after anneal through SPER. Substitutional carbon limits the diffusion and improves the steepness of the annealed dopant profiles [3,4]. However, the PAI step is a major contributor to implant damage and junction leakage. Using lower implant temperatures to create an α-layer with carbon is a potential solution to eliminating this Ge step.

The damage and amorphous layer formation properties of a 6 keV 1×10^{15} cm^{-2} carbon implant were investigated using spot beam and ribbon beam. The ribbon beam current density was approximately 4x lower than the spot beam. Additionally, within each ion beam mode the wafer scan velocity was varied by a factor of 3. This resulted in a normalized effective dose rate variation as listed in table 1 below.

Table 1: Effective dose rate variation using spot or ribbon beam and scan velocity variation

Normalized effective Dose rate		
	Spot beam	Ribbon beam
Low scan velocity	1	0.23
High scan velocity	0.33	0.072

The substrate chiller T was further varied between +15°C and - 50 °C.

Figure 1 below shows HR-XTEM data for a spot beam implant at high scan velocity. As can be seen, the temperature has a significant effect on the α-layer formation. At +15°C a highly damaged layer is formed, with very incomplete amorphization. At -20 °C a continuous 21 nm α-layer is formed and at -50 C the thickness of this continuous α-layer is further increased to 25 nm.

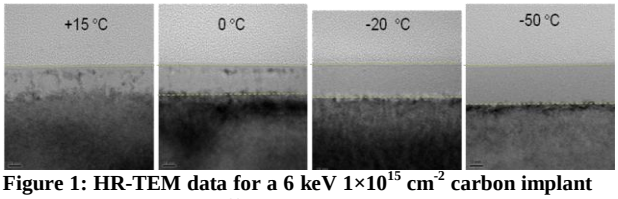

Figure 1: HR-TEM data for a 6 keV 1×10^{15} cm^{-2} carbon implant using a spot beam at different substrate chiller T between +15 °C and -50 °C.

The effect of lower temperature is to suppress interstitial-vacancy recombination or dynamic annealing during implant. The increased thickness at -50 °C is most likely because an α-layer is formed earlier in the implant process and the additional damage generated from that point onward adds to the final thickness rather than escape beyond the a/c interface.

Concluding, replacing a Ge PAI step with a cold C implant appears feasible and the optimal implant temperature to obtain the desired c/α interface position commensurate with other process requirements will have to be carefully determined. Figure 2 shows additional HR-XTEM data from the two extremes of the normalized dose rates listed in Table I.

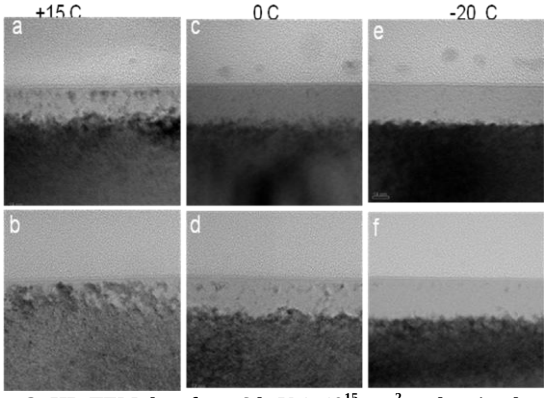

Figure 2: HR-TEM data for a 6 keV 1×10^{15} cm^{-2} carbon implant for a spot beam at low scan velocity (top row) and a ribbon beam at high scan velocity (bottom row) at three implant temperatures.

The effective dose rate difference between these two cases is a factor of 15. At +15 °C there is a clear difference, with the higher effective dose rate fig. 2(a) creating significantly more extended damage than the lower dose rate case, fig. 2(b). At 0 °C there is still a difference but smaller and at -20 C both dose rates produce a similar 20 nm α-layer. The interface roughness of the low dose rate case, fig 2(f), may be somewhat higher but it is difficult to quantify this meaningfully from a TEM picture. Table 2 shows that the SPV signal can track the pre-α layer damage variation with temperature.

Table 2: SPV signal variation for the conditions shown in fig 2

	+15 °C		**0 °C**		**-20 °C**	
	Spot	Ribbon	Spot	Ribbon	Spot	Ribbon
SPV ($\times10^7$ cm^{-3})	1.38	0.59	1.54	0.64	1.54	1.19

Despite a 15x dose rate difference, at -20 °C very similar damage is produced. This behavior can be understood in terms of the critical dose for amorphization. Above the critical dose an α-layer is produced, below it a highly defected but crystalline layer results. Crucially, the critical dose for amorphization is a very strong function of specie, energy, current density, dose, and substrate temperature. There is a complicated interplay between all of these parameters, as described in the literature by Goldberg *et al.* [5] and more recently reviewed by Pelaz *et al*. [6] Figure 3 below shows a cartoon, based on these literature results, that applies the concept of critical dose to the data described above. Figure 3 shows two critical dose curves for the beam current densities associated with the two dose rates in figure 2. Below each curve only extended defect formation will occur; above each curve an α-layer will form.

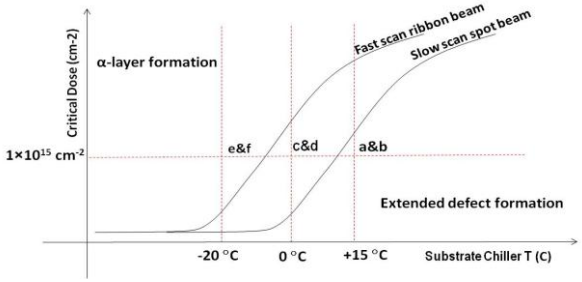

Figure 3: Cartoon illustrating the relationship between beam current density, implant dose and substrate T for a 6 keV 1×10^{15} cm^{-2} carbon implant. Letters refer to the TEM pictures of fig. 2.

At +15 °C, the intersection with the 1×10^{15} cm^{-2} dose (fig. 2 a&b) is below the critical dose curve for both dose rates, but the higher dose rate (a) is much closer to the critical dose curve, and this particular implant condition is therefore much closer to forming an α-layer. At 0 °C, a 1×10^{15} cm^{-2} dose is above the higher dose rate curve, but still below the lower dose rate curve (fig.2c&d). At -20 °C and 1×10^{15} cm^{-2} both sets of implant conditions are above their respective critical dose curves and an α-layer forms for both conditions (fig.2e&f).

It is important to realize that the functional relationship as illustrated in figure 3 will be different for every specie/beam current density combination and therefore in principle specific to individual recipe and implant tool parameters. This sensitivity may easily lead to confusing and/or seemingly contradictory process and device results when the substrate T is lowered indiscriminately.

Dopant diffusion and Activation

Junction formation may benefit further from low implant temperatures by improving dopant activation, limiting diffusion and reducing junction leakage. The α-layer formation may limit channeling as well as improve activation through SPER during anneal. Implant conditions were B 300 eV 1×10^{15} cm^{-2} and B 2 keV 3×10^{15} cm^{-2} for p-type S/D and contact formation, and As 2 keV 1×10^{15} cm^{-2} and As 20 keV 3×10^{15} cm^{-2} for n-type S/D and contact formation.

Table 3: As-implanted α-layer thickness and SPV signal at +15°C and -50 °C substrate chiller temperature

	+15 °C		-50 °C	
	α (nm)	**SPV (C/m^3)**	**α (nm)**	**SPV (C/m^3)**
B 300 eV 1×10^{15} cm^{-2}	**0**	**436**	**2.3**	**428**
B 2 keV 3×10^{15} cm^{-2}	**3.2**	**149×10^2**	**4.7**	**108×10^2**
As 2 keV 1×10^{15} cm^{-2}	**5.8**	**1.33×10^2**	**5.9**	**1.11×10^2**
As 20 keV 3×10^{15} cm^{-2}	**40**	**8.46×10^4**	**40**	**10.2×10^4**

The substrate chiller T was varied between +15 °C and -50 °C. All the implants were performed in a high scan velocity, spot beam mode. Table 2 lists the as-implanted α-layer thicknesses as determined from HR-XTEM (not shown) and SPV signals.

At +15 °C the 300 eV B implant did not generate enough excess interstitials to form an α-layer or extended defects noticeable on a HR-XTEM. However, at -50 °C the dynamic annealing and interstitial mobility was sufficiently suppressed to produce a 2.3 nm α-layer. The SPV signal shows a small change. The B 2 keV, on the other hand, did generate an α-layer at both +15 °C and -50 °C, with a 50% increase in layer thickness at -50 °C. Here the SPV signal variation accurately tracked the thickness change.

Arsenic generated as-implanted α-layers for all conditions. Differently from B and C results, the α-layer thickness was now independent of temperature. This may be because the critical dose curve will be shifted to higher temperatures compared to C (see fig. 3). The temperature-dose intersections points will all be well above the critical dose curves. So, even though the onset of amorphization may be earlier at -50 °C, the difference is too small to cause a measurable change in final α-layer thickness. The observed SPV signal changes are believed to reflect changes in α-layer quality.

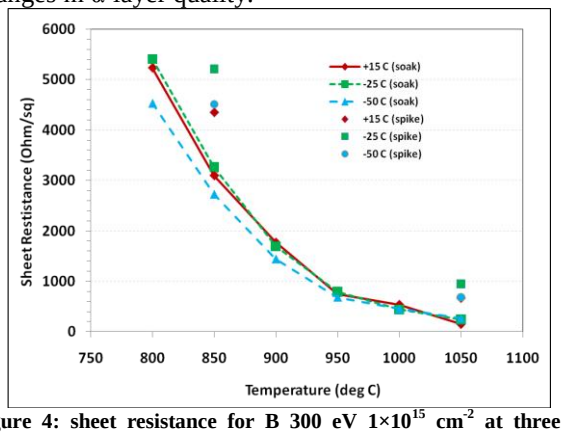

Figure 4: sheet resistance for B 300 eV 1×10^{15} cm^{-2} at three different implant temperatures and after a 10s soak anneal between 800 °C and 1050 °C (lines+markers) as well as a spike anneal at 850 °C and 1050 °C (markers only).

Figure 4 shows the sheet resistance for a B 300 eV 1×10^{15} cm^{-2} implant at three different implant temperatures and after a 10s soak anneal between 800 °C and 1050 °C as well as a spike anneal at 850 °C and 1050 °C. The soak anneal data show very little difference between implants at +15 °C and -25 °C. At -50 C° the R_s is about 15% lower up to 950 °C. The spike anneal values are higher due to the lower thermal budget. As with the soak anneal, there is little difference between +15 °C and -50 °C implant cases. Concluding, although there was a significant

difference in the as-implanted damage signature at these implant temperatures (see table 3) this did not significantly affect activation.

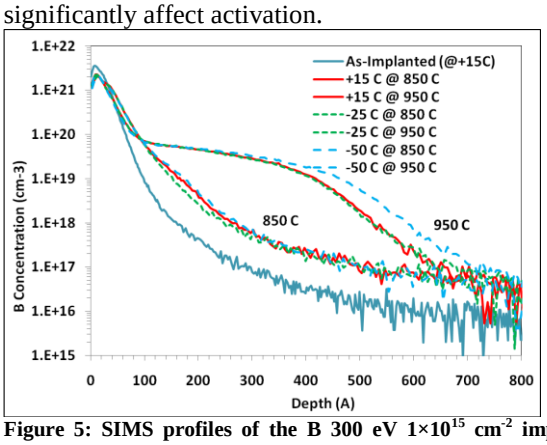

Figure 5: SIMS profiles of the B 300 eV 1×10^{15} cm^{-2} implant after a 10s 850 C and 950 C RTP. Plotted are the as-implanted as well as the profiles for +15 °C, -25 °C and -50 °C implant temperature

Figure 5 shows SIMS profiles for the B 300 eV 1×10^{15} cm^{-2}**,** as-implanted and after a 10 s 850 C anneal**.** The unique design of the iPulsar beam line guarantees a zero energy contamination as-implanted profile. After anneal **t**here is considerable TED at all implant temperatures. At the 5×10^{18} cm^{-3} level the profile moves from 110 Å to 180 Å for -25 °C implant T and to 200 Å for the +15 °C and -50 °C. After 10 s 950 °C SIMS profiles display considerably more diffusion with an x_j of 440 Å for +15 °C and -25 °C and 520 Å for -50°C. At either anneal condition the lowest implant temperature did **not** produce the shallowest profile. The B 2 keV 3×10^{15} cm^{-2} implant (not shown) displayed a very similar soak anneal behavior.

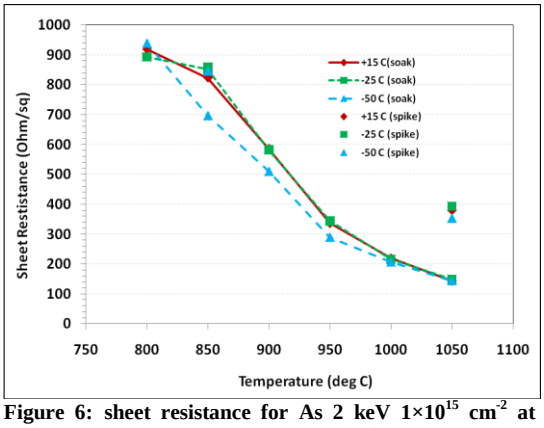

Figure 6: sheet resistance for As 2 keV 1×10^{15} cm^{-2} at three different implant temperatures and after a 10s soak anneal between 800 °C and 1050 °C (lines+markers) as well as a spike anneal at 850 °C and 1050 °C (markers only).

Figure 6 shows anneal results for the As 2 keV 1×10^{15} cm^{-2} implant. The trend is very similar to the B 300 eV, with the lowest implant temperature a 15%-20% lower R_s up to 1000 °C.

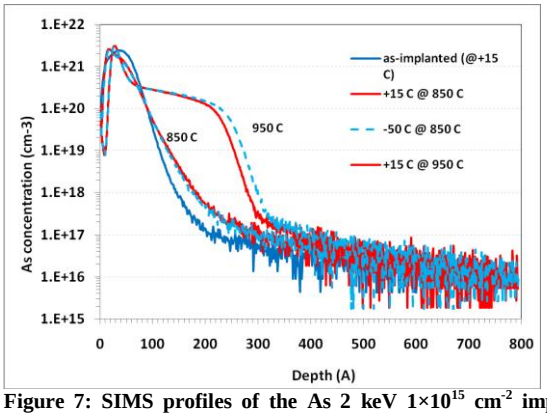

Figure 7: SIMS profiles of the As 2 keV 1×10^{15} cm^{-2} implant after a 10s 850 °C and 950 °C RTP. Plotted are the as-implanted as well as the profiles for +15 °C and -50 °C implant temperature.

As with B, the lowest implant temperature produced a slightly deeper annealed profile at 950 C. The As 20 keV 3×10^{15} cm^{-2} soak anneal behavior did not show any implant temperature dependence (not shown).

CONCLUSIONS

The effects of cold implant and ion beam dose rate were investigated using the unique properties of the iPulsar high current ion implanter. It was shown that by reducing the substrate chiller temperature to at least -20 °C a continuous α-layer can be formed using a low energy C implant. This may lead to the possible elimination of a Ge PAI step, thereby improving implant damage induced device leakage. Lowering the substrate chiller temperature further to -50 °C improved the activation of very low energy B and As implants by up to 20%. However, the corresponding diffused dopant profiles were similar, with the deepest profiles at -50 C.

More generally, it was shown that the relationship between implant recipe details, implant method and substrate temperature is such that careful temperature optimization of each separate implant step may be required to get the maximum benefit. This optimum may not be at the lowest temperature.

REFERENCES

1. M.S. Ameen, M.A Harris, C Huynh, R.N. Reece, Proc. IIT 2008, p.30.
2. P. Kopalidis, Z. Wan, E. J Collart, *these proceedings*
3. B.J. Pawlak et al, Appl. Phys. Lett **89**, 062102 (2006)
4. B.J Pawlak et al, Appl. Phys. Lett. **89**, 062110 (2006)
5. R.D Goldberg, J.S. Williams, R.G.Elliman, Nucl. Instrum. Method. Phys. Res. B 106, 242 (1995)
6. L.Pelaz, L.A. Marques, and J. Barbolla, J.Appl.Phys. **96,** 5947, 2004.